

# A collisional-radiative model including sublevel parameters (CRISP) for H-alpha radiation

E L Foley<sup>1,2</sup> and F M Levinton<sup>2</sup>

<sup>1</sup> Princeton Plasma Physics Laboratory, Princeton University, Princeton, NJ 08543, USA

<sup>2</sup> Nova Photonics, Inc., Princeton, NJ 08540, USA

E-mail: [foley@novaphotonics.com](mailto:foley@novaphotonics.com)

Received 3 October 2005, in final form 13 November 2005

Published 19 December 2005

Online at [stacks.iop.org/JPhysB/39/443](http://stacks.iop.org/JPhysB/39/443)

## Abstract

We have developed a new kind of collisional-radiative model for a hydrogen beam which could find wide application in fusion-related experiments. The model differs from previously reported models in that it incorporates detailed calculations of the variation with the magnetic field of the transition probabilities and energy levels of all the fine-structure sublevels of the  $n = 1$ ,  $n = 2$  and  $n = 3$  states of hydrogen. This technique is termed CRISP, for collisional-radiative including sublevel parameters. The model can treat separately all 18 sublevels of the  $n = 3$  level, all 8 sublevels of the  $n = 2$  level and both 2 sublevels of the  $n = 1$  level. In this paper, we describe the model, which includes the effects on electronic level populations of collisional processes with background gas as well as radiative transitions. The dependence of the radiative transition terms in the collisional-radiative model on background fields is calculated using the perturbation theory and includes the fine structure of the transitions as well as the Zeeman and motional Stark effects. We also present results which agree well with experimental data for an enhanced laser-induced fluorescence signal seen from a hydrogen neutral beam in a perpendicular applied magnetic field of 0–10 mT with a background of neutral gas. This work may have application in the measurement of magnetic fields in environments that are not appropriate for magnetic probes. We expect the CRISP model approach to have application in calibration of motional Stark effect diagnostics on existing fusion experiments, and an extension of the modelling may enable an alternative motional Stark effect measurement of the magnetic field magnitude and direction on many devices.

## 1. Introduction

The H-alpha ( $n = 3$  to  $n = 2$ ) transition in hydrogen is of fundamental interest in astrophysics, laboratory science and industrial applications, and has been extensively studied (cf Olson

(1981), Goldsmith *et al* (1978) and Hamatani *et al* (2002)). In much of this work, the fine structure of the transition is ignored, as the closely spaced lines usually cannot be resolved due to Stark or Doppler broadening. In some situations, it is possible, and even important, to consider the fine structure (Lavrov and Pipa 2002). In the case of neutral atomic hydrogen in an energetic beam, studied in basic atomic physics (Cornet *et al* 1984, Claeys *et al* 1985) and fusion energy diagnostic contexts (Foley and Levinton 2004), the fine structure can sometimes be resolved.

As a neutral beam moves through a perpendicular magnetic field, the beam atoms perceive in their reference frame a Lorentz electric field,  $E_L = v \times B$ , which causes the energy levels to be split, and the wavefunctions modified, due to the motional Stark effect (MSE) and the Zeeman effect in addition to the fine structure due to the spin-orbit coupling and the Lamb shift. The polarization aspects of the motional Stark effect have been exploited to measure magnetic field pitch angle in fusion-energy relevant plasma experiments (Levinton *et al* 1989). Here, magnetic fields and beam energies are large enough to make the line splitting due to MSE dominate, and most of the modelling that has been done to predict emission from the beam has neglected the other effects (Mandl *et al* 1993, Anderson *et al* 1993, Hutchinson 2002). This modelling has used a ‘bundle- $n$ ’ approach—assuming that radiative lifetimes are the same for all sublevels of the  $n = 2$  and  $n = 3$  states in the hydrogen neutral beam, and that all the Stark split levels are statistically populated. Some previous work (Boileau *et al* 1989) has treated the Stark–Zeeman levels independently, and calculated intensities accordingly, but has not taken fine structure into account, or considered the variation of the sublevel parameters in a magnetic field gradient.

The work described in this paper treats all the sublevels of the  $n = 1$  to  $n = 3$  states in a hydrogen neutral beam passing through background magnetic or electric fields, with optional laser excitation from the  $n = 2$  levels to the  $n = 3$  levels. The evolution of the states in field is calculated, and the dependence of the radiative transition parameters between states on field is determined and included in a collisional-radiative model that tracks the population of the sublevels in the beam as it passes through a field gradient. The geometry of the beam, magnetic field, viewing angle and laser polarization are all taken into account. In this work, the beam is considered to travel through a background of neutral hydrogen ( $H_2$ ) gas, and it is seen that the full sublevel treatment is vital for the correct understanding of a laser-induced fluorescence experiment that the model is used to interpret.

## 2. Quantum mechanics calculations

The  $n = 1$ ,  $n = 2$  and  $n = 3$  states of atomic hydrogen in a neutral beam were studied in background magnetic and electric fields including the Stark effect, the motional Stark effect, the Zeeman effect and the fine structure. The known unperturbed eigenfunctions in the  $|l, s, m_l, m_s\rangle$  representation were used as basis states for the perturbed solution. A similar calculation for the  $n = 2$  and  $n = 3$  states of beam hydrogen in a background magnetic field has been described in great detail elsewhere (Souw and Uhlenbusch 1983, Fiksel *et al* 2003), and will simply be outlined here.

The fine structure of the  $n = 2$  and  $n = 3$  levels in atomic hydrogen is shown in figure 1, in  $l_j$  notation, where  $j = l + s$  is the total angular momentum quantum number. Here, the Lamb shift and the spin-orbit coupling are included, but the effects of hyperfine structure are not. The figure also shows the allowed transitions between the  $n = 3$  states and the  $n = 2$  states in the absence of any external fields.

A beam of neutral hydrogen atoms was considered to be moving at an arbitrary angle to background magnetic and electric fields. A  $2n^2 \times 2n^2$  Hamiltonian matrix was written for

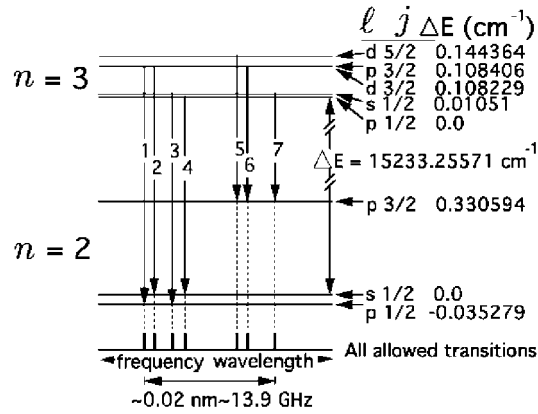


Figure 1. Diagram showing fine structure and allowed transitions for hydrogen H-alpha line.

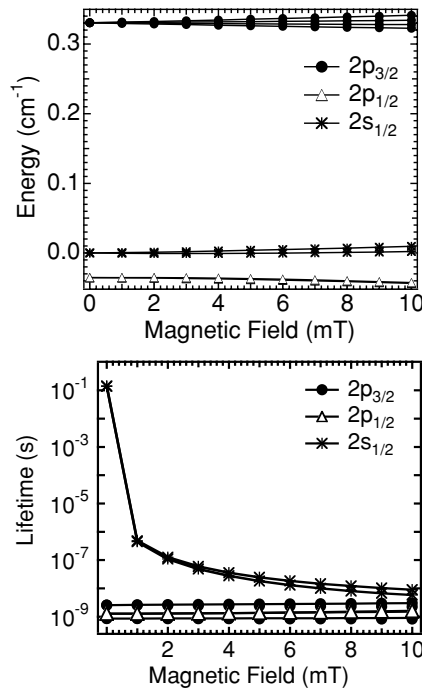
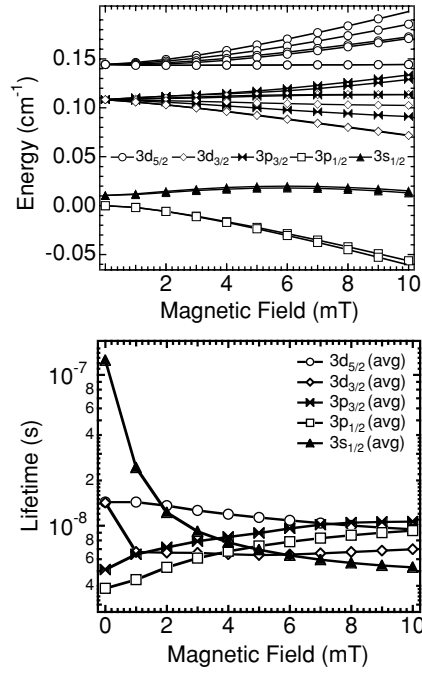


Figure 2. Top: calculated energy levels of beam hydrogen  $n = 2$  states versus the magnetic field for 30 kV beam. Bottom: calculated lifetimes of beam hydrogen  $n = 2$  states versus the magnetic field for 30 kV beam.

each  $n$  level, including dependence on applied fields, and diagonalized to find the eigenvalues (energy levels) and eigenvectors (wavefunctions in terms of coefficients for basis set of wavefunctions) at any given field. From the eigenvectors, spontaneous transition rates between the levels were calculated and from these the lifetime of each state was determined. Figure 2 shows the variation of the energy levels and lifetimes of each of the  $n = 2$  states in a 30 kV atomic hydrogen beam versus the applied perpendicular magnetic field.

In the absence of applied fields, spontaneous transitions from the  $2s_{1/2}$  state to ground are forbidden. The  $2s_{1/2}$  state is metastable, and it has an extremely long lifetime of 0.14 s, decaying

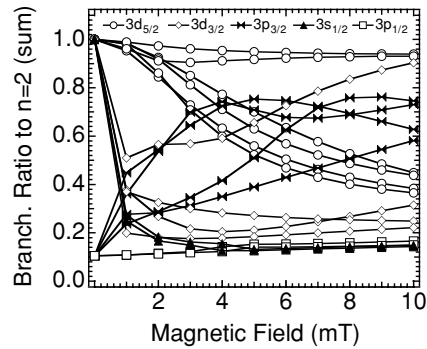


**Figure 3.** Top: calculated energy levels of beam hydrogen  $n = 3$  states versus magnetic field for a 30 kV beam. Bottom: calculated lifetimes of beam hydrogen  $n = 3$  states versus the magnetic field for a 30 kV beam.

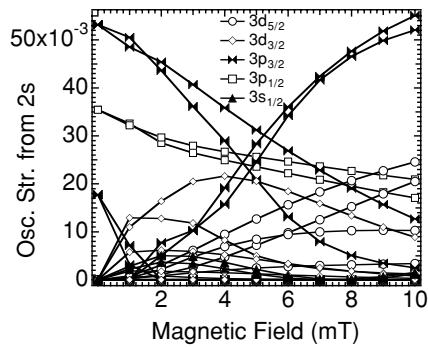
only through a two-photon transition to ground. In the presence of some electric field, in this case a motional Stark field from the atom's motion through a background magnetic field, the wavefunctions are distorted, and the state that the  $2s$  state evolves into has some overlap with the zero-field  $2p$  states. Thus, an electron which in the absence of field was in the  $2s_{1/2}$  state will in the presence of field have some probability amplitude to transition through a single-photon transition to ground, and its lifetime drops rapidly with the applied field. Figure 3 shows the calculated energy levels and lifetimes for the  $n = 3$  states. Note that some are so close in energy that they overlap in the figure so all 18 states are not clearly distinguishable. Also note that the  $3s_{1/2}$  state is comparatively long lived at zero field. As such it can be considered quasimetastable, and like the metastable  $2s_{1/2}$  state, its lifetime diminishes rapidly as the field grows.

Figure 4 shows the calculated branching ratios from each of the  $n = 3$  states to the sum of all the  $n = 2$  states for a 30 kV beam. In order to account for laser-induced excitation from  $n = 2$  to  $n = 3$ , a feature of the experiment described later in this paper and used for comparison to the model, the laser pumping term for each possible transition was calculated (Griem 1997). This term, given in equation (1), where  $W$  is the laser pumping rate in Hz,  $r_0$  is the classical electron radius,  $I(\omega_{ul})$  is the laser beam intensity per unit area per unit angular frequency and  $\omega_{ul}$  is the angular frequency of the transition, is dependent on the oscillator strength of the transitions. Figure 5 shows the calculated oscillator strength for laser excitation from the two  $2s_{1/2}$  states to all the  $n = 3$  states for a 30 kV beam passing perpendicularly through a magnetic field, with the laser polarization parallel to the induced electric field.

$$W(B) = \frac{2\pi^2 r_0 c f_{lu}(B) I(\omega_{ul})}{\hbar \omega_{ul}} \quad (1)$$



**Figure 4.** Calculated sum of branching ratios from each  $n = 3$  state to all  $n = 2$  states for a 30 kV beam.



**Figure 5.** Calculated oscillator strength for  $y$ -polarized laser from  $2s_{1/2}$  states to all  $n = 3$  states versus the magnetic field.

### 3. Collisional-radiative including sublevel parameters (CRISP) model

Experimentally observed H-alpha collisionally induced fluorescence (CIF) and laser-induced fluorescence (LIF) signals from a hydrogen neutral beam will depend on the populations of the excited states. These populations can change through collisional processes: increasing by collisions with background gas which excite electrons from lower levels, or neutralize ions into the level of interest, and decreasing by collisions that take electrons to other levels, or ionize the atom. The populations can also change via radiative processes: decreasing by radiation of electrons to lower levels, either spontaneous or stimulated emission, or by laser excitation to higher levels, and possibly increasing by laser-induced excitation from lower levels. It was seen in the previous section that many of the radiative transition parameters vary significantly with the magnetic field from 0 to 10 mT. Additionally, an observed signal is dependent on the total branching ratio from  $n = 3$  to  $n = 2$ , which varies with the magnetic field. In the regime studied here, the radiative lifetimes of the states are on the order of the collision times, so all the aforementioned processes compete and therefore must be taken into account for an accurate description of the system. The confluence of effects in this regime leads the analysis to be maximally complicated. The collisional-radiative model described here predicts the CIF and LIF signals from a hydrogen neutral beam in a perpendicular magnetic field by solving the differential equations governing the state populations in the beam, using collisional cross

$$\begin{aligned}
 & \text{change in population of atomic level } i \text{ with distance along beam path} \\
 & \text{beam velocity} \quad v_b \frac{dn_i}{dx} = - \left[ I_i + \sum_{j>i} E_{ij} + \sum_{j<i} D_{ij} + \sum_{j<i} A_{ij} + W_{ij} \right] n_i \\
 & \quad + \left[ \sum_{j<i} E_{ji} + \sum_{j>i} D_{ji} + \sum_{j>i} A_{ji} + W_{ji} \right] n_j + R_i n_{ions}
 \end{aligned}$$

ionization rate from state i      de-excitation rate from i to j      optical pumping rate  
 excitation rate from i to j      radiative decay rate from i to j      population in level i  
 de-excitation rate from j to i      optical pumping rate      population in level j  
 excitation rate from j to i      radiative decay rate from j to i      recombination rate into state i

Figure 6. Form of differential equation solved in collisional-radiative model.

sections from the literature, and radiative transition parameters calculated with the quantum mechanical model of the previous section.

Figure 6 shows a general example of the type of differential equation solved in the CRISP model. Such an equation is written for the time derivative of the population for each level included in the model. For the beam moving at constant velocity  $v_b$ , the spatial derivative multiplied by  $v_b$ , as shown in figure 6, is equivalent to the time derivative. A full description of the system includes a set of such coupled differential equations, one for each state, all of which depend on the population of the other states. Here, the set consists of 29 coupled differential equations, one for each of the sublevels of the  $n = 1$ ,  $n = 2$  and  $n = 3$  states, and one for the ions. The rates for the collisional processes depend on the density of background target particles ( $n$ ), the cross section for the process ( $\sigma$ ) and the relative velocity ( $v_{rel}$ ) as  $\text{Rate} = n\sigma v_{rel}$ . The last term shown in the collisional-radiative model equation of figure 6 represents recombination of ions into a given state. This term should be neglected in the case of a background magnetic field which is large enough to sweep ions out of the beamline before they can be re-neutralized.

Cross sections for collisional neutralization, ionization, excitation and de-excitation for 30 kV hydrogen atoms (or ions, as appropriate) on a background of  $H_2$  gas were taken from experimentally determined values from the literature when available. Table 1 shows these cross sections along with references. Some cross sections needed for the code, especially sub-level specific cross sections for levels other than the s levels, were not available. In these cases, the cross sections were estimated from other available values that were presumed to be similar. For example, the cross section for collisional excitation from the  $2s_{1/2}$  to the  $3s_{1/2}$  level was available, but no other sublevel-specific cross sections were available for the  $n = 2$  to  $n = 3$  collisional excitation. In this case, all the cross sections for collisional excitation from any  $n = 2$  state to any  $n = 3$  state were taken to be the same as this value. Also, de-excitation cross sections between levels were assumed to be equal to the excitation cross sections for the same levels. For states with multiple sublevels, the individual sublevel cross sections were calculated to give agreement with the reference value for the total. All the collisional cross sections were assumed to be constant with the varying magnetic field.

Cross sections for collisional mixing of sublevels were not available in the literature, so the effect of mixing was considered by comparing the case of no collision-induced transitions between sublevels of the same  $n$  to the case of collisional mixing with a maximum theoretical cross section for collisional mixing, which in the case of neutral hydrogen gas was taken to be roughly the size of the molecule, or  $10^{-16} \text{ cm}^2$ .

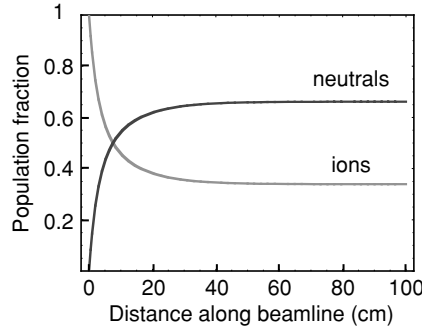


**Figure 7.** Calculated population levels for ions and  $n = 1$  with no applied field or no laser. Plot shows maximum equilibrium fraction with 10 mTorr in the beamline.

**Table 1.** Cross sections for given processes at given energies for impact on  $H_2$  gas.

Level	Cross section ( $\sigma$ ) ( $cm^2$ )	References	Energy (kV)
Electron capture by ion into			
1s	$1.6 \times 10^{-16}$	Stier and Barnett (1956)	30
2s	$1 \times 10^{-17}$	Barnett (1990)	30
2p	$2.5 \times 10^{-17}$	Barnett (1990)	30
3s	$8 \times 10^{-18}$	Hughes <i>et al</i> (1970)	30
3p	$2 \times 10^{-18}$	Hughes <i>et al</i> (1970)	30
3d	$5 \times 10^{-19}$	Hughes <i>et al</i> (1970)	30
Ionization from			
1s	$8 \times 10^{-17}$	Stier and Barnett (1956)	30
2s	$4 \times 10^{-16}$	Gilbody and Corr (1974)	30
Excitation from $n = 1$ to			
2s	$1 \times 10^{-17}$	Hughes <i>et al</i> (1972)	25
2p	$2 \times 10^{-17}$	Hughes <i>et al</i> (1972)	25
3s	$1.6 \times 10^{-17}$	Hughes <i>et al</i> (1972)	30
3p	$2 \times 10^{-17}$	Hughes <i>et al</i> (1972)	30
3d	$8 \times 10^{-18}$	Hughes <i>et al</i> (1972)	30
Excitation from $nl = 2s$ to			
3s	$1.2 \times 10^{-17}$	Hill <i>et al</i> (1980)	25

#### 4. CRISP model results

Examples of results from the CRISP model are shown in figures 7 and 8. Figure 7 shows the ion and ground state hydrogen neutral population fractions of a 30 kV beam that is given the initial condition of 100% ion population at  $x = 0$  that is passing through a background of 10 mTorr of  $H_2$  gas, enough to reach equilibrium neutral population. Here, the final neutral fraction of 66% is in good agreement with the value of  $\sim 70\%$  reported by Stier and Barnett (1956) at 30 kV, as is the integrated line density required to achieve it.

Figure 8 shows the total population of the  $n = 2$  and  $n = 3$  sublevels as they propagate down a beamline with the pressure profile of figure 9. Noting that the y-axes for the plots in

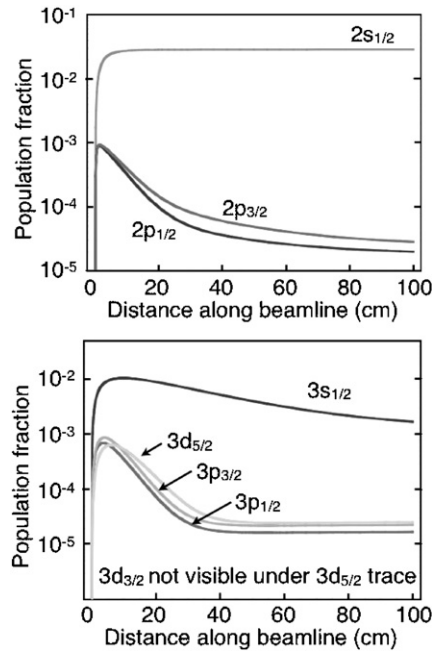


**Figure 8.** Calculated population levels with no applied field or laser. Top: level  $n = 2$ . Bottom: level  $n = 3$ .

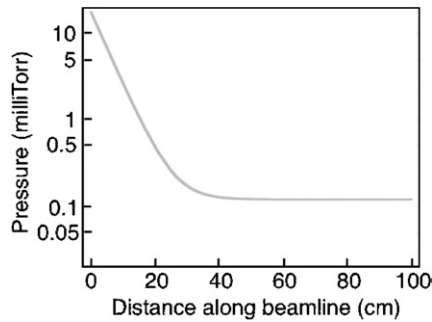


**Figure 9.** Pressure profile along beamline used in CRM.

figure 8 are on a log scale, it is clear that in the absence of fields, the population of the  $n = 2$  level (top) shows a significant imbalance between different states: the  $2s$  state population is roughly three orders of magnitude greater than the  $2p$  population at 100 cm. This can be understood by considering the  $2s$  state radiative lifetime, which is 0.14 s in the absence of applied fields. As discussed in section 2, the state is metastable. Because of the long radiative lifetime, the actual  $2s$  state lifetime is determined by collisions. The final  $2s$  metastable fraction in figure 8 for the pressure profile of figure 9 is  $\sim 2\%$ , which is consistent with the previously measured value of 1.8% (Gilbody and Corr 1974) for passage of an ion beam through a molecular hydrogen background of 0.1 Torr cm (the integral of the gas density profile of figure 9). Measurements presented in Gilbody and Corr (1974) reveal that an ion beam at 30 kV yields the maximum possible  $2s$  metastable fraction for beam energies in the range of 5–500 kV on  $H_2$  gas. In the  $n = 3$  population levels, there is a similar trend, though it is not as pronounced. The  $3s$  lifetime

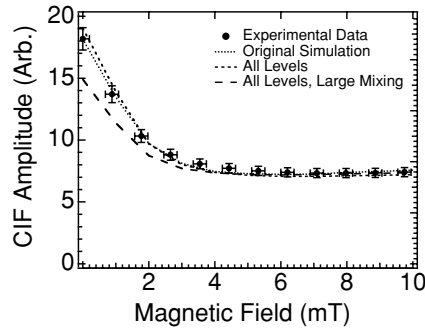


**Figure 10.** Comparison of data and simulation for total collisionally induced fluorescence signal. All are plotted on the same scale.

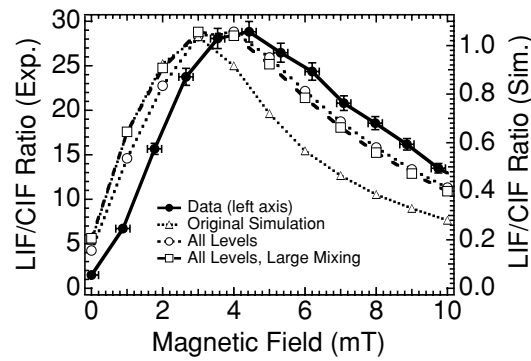


**Figure 11.** Comparison of data and simulation for LIF/CIF ratio. All are scaled to match at the peak.

of  $\sim 150$  ns is more than an order of magnitude larger than the 3p and 3d lifetimes ( $\sim 5$  ns and  $\sim 15$  ns, respectively) in the absence of field, and as such it can be said to be quasimetastable. The population of the 3s level grows to nearly two orders of magnitude more than that of the 3p and 3d levels by the 100 cm viewing region. Note that the initial rise of all population levels is due to the higher pressure closer to  $x = 0$ , and the level populations decay as the pressure decreases.

In figure 8, the sublevels of  $n = 2$  and  $n = 3$  are grouped into sets based on their  $l_j$  values at zero field. The CRISP simulation can be run to retain this grouping even as magnetic fields are applied. The advantage of this approach is that it significantly reduces the number and complexity of the equations solved by the model, as the 18 states in  $n = 3$  are simplified to five sets, the eight states of  $n = 2$  are reduced to three and the two  $n = 1$  states are treated as one. The disadvantage is some loss of information, and the two versions of the model are compared to each other and to an experimental situation in figures 10 and 11.

## 5. Comparing CRISP model to experiment

The CRISP model was used to interpret the results of a laser-induced fluorescence experiment on a neutral hydrogen beam passing through a weak magnetic field. In this experiment, which is described in detail by Foley and Levinton (2005), fluorescence of the full H-alpha spectrum

was observed with and without a laser tuned to excite fluorescence from  $n = 2$  to  $n = 3$ . When a magnetic field was applied perpendicular to the beamline, the collisionally induced fluorescence signal from the beam at the peak of the field was seen to drop rapidly, to about half of the no-field level, as the field varied from 0 to 10 mT, as shown in figure 10. Meanwhile, the total laser-induced fluorescence signal was seen to increase dramatically over the same field range, reaching a peak at around 4 mT, and then dropping as the field continued to increase. LIF data from 0–10 mT are shown in figure 11.

The CRISP model code was applied to this experiment with good results, as shown in figures 10 and 11. The CIF signal is seen to drop as the lifetime of the  $3s_{\frac{1}{2}}$  state drops rapidly, and fewer electrons build up in the  $n = 3$  level. The LIF signal increases because in this experiment, the zero-field signal was dominated by LIF excited from the metastable  $2s_{\frac{1}{2}}$  with its surfeit of electrons. At zero field, the laser can excite transitions from  $2s_{\frac{1}{2}}$  to  $2p_{\frac{1}{2}}$  and  $2p_{\frac{3}{2}}$  only, but when field is applied and the states mix, transitions become allowed from  $2s_{\frac{1}{2}}$  to  $3s_{\frac{1}{2}}$ ,  $3d_{\frac{3}{2}}$  and  $3d_{\frac{5}{2}}$  as well, giving more lines and more signal. Also, the branching ratio from  $3p_{\frac{3}{2}}$  to all  $n = 2$  states increases significantly. There may also be an effect which is not accounted for in the CRISP model—of  $2s_{\frac{1}{2}}$  electrons transitioning to the nearby and overlapped  $2p_{\frac{1}{2}}$  state as they pass into the magnetic field (Brouillard and Van Wassenhove 1974). The  $2s_{\frac{1}{2}}-3d_{\frac{3}{2}}$  transition is experimentally indistinguishable from the  $2p_{\frac{1}{2}}-3d_{\frac{3}{2}}$  transition. This effect may account for the additional enhancement seen in the data.

## 6. Conclusions

The CRISP model code described in this article is shown to match well to experimental data in a regime in which a code that did not explicitly account for the variation of fine-structure level parameters would not have. This type of model may have wide application on fusion experiments. Collisional-radiative modelling for hydrogen in the plasma edge could benefit from the approach, as could motional Stark effect hydrogen beam-based diagnostics. Calibration data for the motional Stark effect on several experiments have yielded line spectra for beam-into-neutral-gas studies that are not consistent with full sublevel mixing (Levinton 1996, Levinton *et al* 1997), but have never been explained. The extension of the CRISP model to higher magnetic field could yield insight. A further extension of the CRISP model to a background of plasma could be useful for the many fusion-relevant experiments which are now operating at fields of much less than 1 T (Ono *et al* 2000, Fonck 1996, Dexter *et al* 1991, Sankar *et al* 1993, Cox 1999, Wang *et al* 2003) where it can be important to include the effects of fine structure in the Stark spectrum. A high-field, plasma background CRISP model may find application in developing a technique for the motional Stark effect diagnostic on high-field machines. Such detailed modelling could reveal a spectroscopic technique for determining pitch angle from line spacing rather than polarization, and this would greatly simplify measurements in harsh environments, where mirror damage will affect polarization. Successful extension of the CRISP model to other applications may benefit from further refinements, such as explicit calculation of the collision cross sections as they vary with sublevels, and inclusion of the quadratic Stark effect.

## Acknowledgments

E L Foley gratefully acknowledges the support of a Hertz Foundation Graduate Fellowship. This work is supported under US Department of Energy grant no. DE-FG02-01ER54616. The authors would like to thank E Valeo, S Suckewer, W Happer and E Synakowski for useful discussions.

## References

- Anderson H, von Hellermann M G, Hoekstra R, Horton L D, Howman A C, Konig R W T, Martin R, Olson R E and Summers H P 1993 *Plasma Phys. Control. Fusion* **35** 1373–4
- Barnett C F 1990 Atomic data for fusion vol 1: collisions of H, H<sub>2</sub>, He, and Li atoms and ions with atoms and molecules *Technical Report* 6086 ORNL
- Boileau A, von Hellermann M, Mandl W, Summers H P, Weisen H and Zinoviev A 1989 *J. Phys. B: At. Mol. Opt. Phys.* **22** L145–52
- Brouillard F and Van Wassenhove G 1974 *J. Phys. B: At. Mol. Phys.* **7** 2308–14
- Claeys W, Cornet A, Lorent V and Fussen D 1985 *J. Phys. B: At. Mol. Phys.* **18** 3667–72
- Cornet A, Claeys W, Lorent V, Jureta J and Fussen D 1984 *J. Phys. B: At. Mol. Phys.* **17** 2643–54
- Cox M 1999 *Fusion Eng. Des.* **46** 2–4 397–404
- Dexter R N, Kerst D W, Lovell T W, Prager S C and Sprott J C 1991 *Fusion Technol.* **19** 131–9
- Fiksel G, Den Hartog D J, Ivanov A A and Lizunov A A 2003 Calculation of the optical transition intensity and energy level splitting for general conditions of the motional Stark effect diagnostic *Technical Report* 2003–29 (Budker Institute of Nuclear Physics)
- Foley E L and Levinton F M 2004 *Rev. Sci. Instrum.* **75** 3462–4
- Foley E L and Levinton F M 2005 *J. Appl. Phys.* **98** 093101
- Fonck R 1996 *Bull. Am. Phys. Soc.* **41** 1400
- Gilbody H B and Corr J L 1974 *J. Phys. B: At. Mol. Phys.* **7** 1953–67
- Goldsmith J E M, Weber E W and Hansch T W 1978 *Phys. Rev. Lett.* **41** 1525–8
- Griem H R 1997 *Principles of Plasma Spectroscopy* (Cambridge University Press: UK) p 21
- Hamatani H, Crawford W S and Cappelli M A 2002 *Surf. Coat. Technol.* **162** 79–92
- Hill J, Geddes J and Gilbody H B 1980 *J. Phys. B: At. Mol. Phys.* **13** 951–58
- Hughes R H, Petefish H M and Kisner H 1972 *Phys. Rev. A* **5** 2103–06
- Hughes R H, Stigers C A, Doughty B M and Stokes E D 1970 *Phys. Rev. A* **1** 1424–32
- Hutchinson I H 2002 *Plasma Phys. Control. Fusion* **44** 71–82
- Lavrov B P and Pipa A V 2002 *Opt. Spectrosc.* **92** 647–57
- Levinton F M 1996 *Atomic Processes in Plasmas* ed A L Osterheld and W H Goldstein (New York: AIP) pp 143–50
- Levinton F M, Batha S H and Zarnstorff M C 1997 *Rev. Sci. Instrum.* **68** 926–9
- Levinton F M *et al* 1989 *Phys. Rev. Lett.* **63** 2060
- Mandl W, Wolf R C, von Hellermann M G and Summers H P 1993 *Plasma Phys. Control. Fusion* **35** 1373–94
- Olson G L 1981 *Astrophys. J.* **248** 1021–30
- Ono M *et al* 2000 *Nucl. Fusion* **40** 557–61
- Sankar M K V *et al* 1993 *J. Fusion Energy* **12** 303–10
- Souw E K and Uhlenbusch J 1983 *Physica B, C* **122** 353–74
- Stier P M and Barnett C F 1956 *Phys. Rev.* **103** 896–907
- Wang Y, Zeng L and He Y X 2003 *Plasma Sci. Technol.* **5** 2017–22